# Online Determination of GNSS Differential Code Biases using Rao-Blackwellized Particle Filtering

Benjamin Reid[(1)]

(1) University of New Brunswick, Fredericton, Canada; e-mail: breid.phys@gmail.com; ben.reid@unb.ca

## Abstract

A-CHAIM is a data assimilation model of the high latitude ionosphere, incorporating measurements from multiple kinds of instruments, including slant Total Electron Content measurements from ground-based Global Navigation Satellite System (GNSS) receivers. These measurements have receiver-specific instrumental biases which must be resolved to produce an absolute measurement, which are resolved along with the ionospheric state using Rao-Blackwellised particle filtering. These instrumental biases are compared to published values and estimation techniques, which show small but consistent systematic differences. The potential cause of these systematic biases is investigated. It is shown that if A-CHAIMs biases agreed with other estimation techniques, the result would be a overestimation of NmF2 ranging from $< 10\%$ during the day to over 20% at night, or a $> 30\%$ overestimation of topside electron density at 800km altitude.

## 1 Introduction

A-CHAIM is a near-real-time data assimilation model of high latitude ionospheric electron density [1]. It uses a particle filter technique to assimilate data from ground-based Global Navigation Satellite System (GNSS) receivers, ionosondes, and satellite-borne altimeters on the JASON-3 and SENTINEL satellites. GNSS receivers are the most widely distributed and numerous, providing slant Total Electron Content (sTEC) measurements along line-of-sight from the satellite to the receiver, usually expressed in TEC Units $1 \times 10^{16} m^{-3}$ (TECU). Using a geometry-free combination of the phase and code observables recorded on each GNSS carrier frequency, the TEC can be related to the observables by (1), where $A = 40.3$, $f_m$ is the $m^{th}$ frequency, $\Delta\phi$ is the difference in the signal carrier phases, $DCB_{rcv}$ and $DCB_{sat}$ are the receiver and satellite differential code biases caused by instrumental delays, and $W$ is a phase-levelling term used to correct an integer ambiguity in the phase-derived TEC using the code observables [2].

$$\text{sTEC} = \frac{1}{A}\left(\frac{f_1^2 f_2^2}{f_1^2 - f_2^2}\right)(\Delta\phi + W + DCB_{rcv} + DCB_{sat}) \quad (1)$$

To be able to obtain an absolute measurement of sTEC these DCBs must be determined. The International GNSS

**Table 1.** Vertical TEC products used to test A-CHAIMs DCB determination. All files were obtained from CDDIS in the IONEX format, except for the Madrigal vTEC maps ∗, which were obtained from the CEDAR Madrigal database.

| ID | Analysis Center |
|----|-----------------|
| cod | Center for Orbit Determination in Europe (CODE) |
| cas | Chinese Academy of Sciences (CAS) |
| esa | European Space Agency (ESA/ESOC) |
| emr | Natural Resources Canada (NRCan) |
| igs | International GNSS Service (IGS) |
| jpl | Jet Propulsion Laboratory (JPL) |
| upc | Universitat Politècnica de Catalunya (UPC) |
| ∗ | Madrigal vTEC Haystack Observatory |

Service (IGS) Analysis Centers produce Global Ionospheric Maps (GIMs) of vertical Total Electron Content (vTEC), distributed in the IONosphere Map EXchange format (IONEX) [3, 4]. Those used in this analysis are summarized in Table 1. The observed sTEC can be converted to vTEC, and compared to the reference map to estimate the DCB. Usually this involves using a thin-shell approximation (**??**), where the ionospheric electron density is assumed to exist entirely in a spherical shell with altitude $h_{shell}$. The mapping function (2) from sTEC to vTEC is dependent on the elevation of the GNSS satellite $e$.

$$vTEC = sTEC \cdot \sqrt{1 - \left(\frac{R_e \cos e}{R_e + h_{shell}}\right)^2} \quad (2)$$

Other groups produce vTEC maps, notably the Madrigal vTEC maps from the Haystack Observatory at MIT [5]. These maps use data from many thousands of receivers, and use a sophisticated bias estimation technique [6]. The same thin-shell bias estimation technique used for the IONEX vTEC maps can also be used with the Madrigal vTEC maps. It would be possible to use any of these techniques to fix the receiver DCBs for A-CHAIM, but relying on an external model for such a critical component of the assimilation has several undesirable consequences. If there were a systematic error in the receiver DCBs, then the residual error would need to be absorbed by the ionospheric model itself. This is why it is preferable to solve for the ionospheric state and the receiver DCBs simultaneously.

## 2 Method

A-CHAIM is vertically parameterized as a semi-Epstein layer, whose shape is controlled by a set of harmonic expansions of several key ionospheric parameters [1]. These parameters include the peak density of the F2 layer, $NmF2$, the altitude of the F2 peak $hmF2$, as well as thickness parameters $H_{Top}$ and $H_{Bot}$ which control the shape of the topside and bottomside ionosphere. The electron density at any point $\vec{r}$ is therefore a nonlinear function $N_e(\mathbf{x}, \vec{r})$ of these harmonic coefficients $\mathbf{x}_s$, which can be described as a vector in a state space $\mathbb{X}_s$. By including the DCBs as parameters to be determined, we add a new set of numbers $\mathbf{x}_{b,1:n} \in \mathbb{X}_b$ to the state. Our new state space is the product of these two sets of parameters (3).

$$\mathbf{x} = (\mathbf{x}_s, \mathbf{x}_b) \in \mathbb{X}_s \times \mathbb{X}_b \qquad (3)$$

A-CHAIM uses a particle filter to perform data assimilation [1]. A particle filter is a Monte Carlo technique with uses a ensemble of sample points, or particles, $\mathbf{X}^i \in \mathbb{X}$ with associated statistical weights $W^i$ to approximate a distribution (5) on $\mathbb{X}$ [7]. The performance of a particle filter is directly dependent on the number of particles in the ensemble. As the number of dimensions of the state space $\mathbb{X}$ increases, the number of particles required to sample the space appropriately increases dramatically [1, 8]. An efficient solution to this problem is Rao-Blackwellised particle filtering, which enables us to solve for the receiver biases analytically [7].

$$p(\mathbf{x}_{s,1:n}, \mathbf{x}_{b,1:n} | \mathbf{y}_{1:n}) = \frac{p(\mathbf{x}_{s,1:n}, \mathbf{x}_{b,1:n}) p(\mathbf{y}_{1:n} | \mathbf{x}_{s,1:n}, \mathbf{x}_{b,1:n})}{p(\mathbf{y}_{1:n})}$$
$$= p(\mathbf{x}_{s,1:n} | \mathbf{y}_{1:n}) p(\mathbf{x}_{b,1:n} | \mathbf{y}_{1:n}, \mathbf{x}_{s,1:n}) \qquad (4)$$

$$\hat{p}(\mathbf{x}_{s,1:n}, \mathbf{x}_{b,1:n} | \mathbf{y}_{1:n}) = \sum_{i=1}^{N} W_n^i \delta_{\mathbf{X}_{1:n}^i}(\mathbf{x}_{s,1:n}, \mathbf{x}_{b,1:n}) \qquad (5)$$

The particles $\mathbf{X}^i$ are sampled from an importance distribution $q(\mathbf{x}_{1:n} | \mathbf{y}_{1:n})$. With the forecast model $f(\mathbf{x}_n | \mathbf{x}_{n-1})$, the probability of transitioning from a state $\mathbf{x}_{n-1}$ to a state $\mathbf{x}_n$, and the likelihood function $p(\mathbf{y}_{1:n} | \mathbf{x}_{1:n})$ allows us to constantly update the weights of our particles $w^i$ with (7).

$$w_1^i(\mathbf{X}_1^i) = \frac{p(\mathbf{X}_{s,1}^i) p(\mathbf{y}_1 | \mathbf{X}_{s,1}^i) p(\mathbf{X}_{b,1}^i | \mathbf{y}_1, \mathbf{X}_{s,1}^i)}{q(\mathbf{X}_{s,1}^i)} \qquad (6)$$

$$w_n^i(\mathbf{X}_{1:n}^i) = w_1^i(\mathbf{X}_1^i) \prod_{k=2}^{n} \frac{f(\mathbf{X}_{s,k}^i | \mathbf{X}_{s,k-1}^i) p(\mathbf{y}_k | \mathbf{X}_{s,k}^i) p(\mathbf{X}_{b,k}^i | \mathbf{y}_k, \mathbf{X}_{s,k}^i)}{q_k(\mathbf{X}_{s,k}^i | \mathbf{X}_{s,k-1}^i)} \qquad (7)$$

In A-CHAIM we assume the DCB behaves as a Gaussian random walk with an average step size $\sqrt{Q_b} = 0.05$ TECU

over a 5 minute assimilation step. While the integrals though the modelled ionosphere to calculate sTEC are nonlinear with respect to the ionospheric state $\mathbf{x}_s$, they are linear with respect to the DCBs. Determining $p(\mathbf{X}_{b,k}^i | \mathbf{y}_k, \mathbf{X}_{s,k}^i)$ for a fixed $\mathbf{X}_s^i$ is therefore a simple linear Gaussian problem, which can be solved with a Kalman filter. Our predicted bias $\hat{\mathbf{x}}_{b,n}$ and bias covariance $\mathbf{P}_n$ are as follows, where $\mathbf{Q}_{b,n}$ is a diagonal process noise covariance chosen to keep $\mathbf{P}_{b,n} \geq (0.05 \text{ TECU})^2$.

$$\mathbf{X}_{b,n}^i = \mathbf{X}_{b,n-1}^i, \quad \mathbf{P}_n^i = \mathbf{P}_{n-1}^i + \mathbf{Q}_{b,n} \qquad (8)$$

The DCBs are simply added to the observations, so the measurement matrix $\mathbf{H}_n^i$ has a similarly simple form.

$$\mathbf{H}_n[i, j] = \begin{bmatrix} 1, & \text{if } rcv(y_n[i]) = rcv(x_{n,b}[j]) \\ 0, & \text{otherwise} \end{bmatrix} \qquad (9)$$

The Kalman gain $\mathbf{K}_n^i$ can therefore be evaluated with the observation error covariance $\mathbf{R}_n^i$. This allows the calculation of the optimal estimator $\hat{\mathbf{X}}_{b,n}^i$ and posterior covariance $\hat{\mathbf{P}}_n^i$.

$$\mathbf{K}_n^i = \mathbf{P}_n^i \mathbf{H}_n^T (\mathbf{R}_n + \mathbf{H}_n \mathbf{P}_n^i \mathbf{H}_n^T)^{-1} \qquad (10)$$

$$\hat{\mathbf{P}}_n^i = (\mathbf{I} - \mathbf{K}_n^i \mathbf{H}_n) \mathbf{P}_n^i \qquad (11)$$

$$\hat{\mathbf{X}}_{b,n}^i = \mathbf{X}_{b,n}^i + \mathbf{K}_n^i (\mathbf{y}_n - \mathscr{H}(\mathbf{X}_{s,n}^i) - \mathbf{H}_n \mathbf{X}_{b,n}^i) \qquad (12)$$

If all $\mathbf{P}_0^i$ are initialized with the same values for each particle, neither the Kalman gain $\mathbf{K}_n^i$, nor any of its constituent matrices have any dependence on $\mathbf{y}_n$ or $\mathbf{X}_n$. As a result, $\mathbf{K}_n^i$ and $\hat{\mathbf{P}}_n^i$ will always be identical for every particle. As we have access to the optimal estimator $\hat{\mathbf{X}}_{b,n}^i$, it would be inefficient to use any other choice of DCB. By setting $\mathbf{X}_{b,n}^i = \hat{\mathbf{X}}_{b,n}^i$, $p(\mathbf{X}_{b,n}^i | \mathbf{y}_{1:n}, \mathbf{X}_{s,n}^i)$ identical for all particles.

We are only interested in the normalized weights $W^i$, we can therefore simplify (7) to (14). By using the Rao-Blackwellised particle filter, choosing $\mathbf{P}_0$ to be identical for every particle, and taking the optimal estimator $\hat{\mathbf{X}}_{b,n}^i$, we are able to factor the DCBs out of the problem entirely.

$$w_1^i(\mathbf{X}_1^i) = \frac{p(\mathbf{X}_{s,1}^i) p(\mathbf{y}_1 | \mathbf{X}_{s,1}^i)}{q(\mathbf{X}_{s,1}^i)} \qquad (13)$$

$$w_n^i(\mathbf{X}_{1:n}^i) = w_1^i(\mathbf{X}_1^i) \prod_{k=2}^{n} \frac{f(\mathbf{X}_{s,k}^i | \mathbf{X}_{s,k-1}^i) p(\mathbf{y}_k | \mathbf{X}_{s,k}^i)}{q_k(\mathbf{X}_{s,k}^i | \mathbf{X}_{s,k-1}^i)} \qquad (14)$$

## 3 Results

A test environment was prepared to perform offline runs of the A-CHAIM system, using data from August 20th, 2022
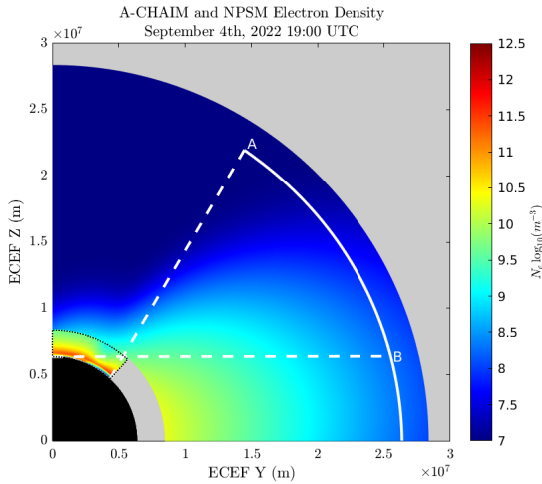
**Figure 1.** A-CHAIM and NPSM electron density at 60°E. The edges of the A-CHAIM domain are indicated with a dotted black line. The solid white line shows the possible positions of a GPS satellite. The dashed line (A) shows the line-of-sight at the extreme southern boundary of A-CHAIM. (B) at $0^o$ elevation from the geographic North pole.

**Table 2.** A summary of the different test runs of the A-CHAIM system. All runs used the full complement of instruments.

| Run | Plasmasphere | vTEC |
|-----|--------------|------|
| ACHAIM (NPSM) | Y | N |
| ACHAIM (no NPSM) | N | N |
| ACHAIM + vTEC | Y | Y |
| ACHAIM + vTEC (HTop) | Y | Y* |

though October 10th, 2022. All of the GNSS and altimeter data used in the tests were those collected in near-real-time by the online assimilation system. In total four separate runs of A-CHAIM were conducted, to attempt to isolate the effect of different model assumptions on the DCBs. The estimated DCBs from each of these runs were saved for every hour of data. The details of these runs are summarized in Table 2. The overall differences in DCBs across all stations are summarized in Figure 2, referenced to the `A-CHAIM (NPSM)` test run.

To attempt to quantify the impact of plasmaspheric plasma on bias estimation, as in Figure 1, two runs were conducted with the usual datasets available to A-CHAIM. One test run included a plasmaspheric correction using the Neustrelitz plasmasphere model (NPSM) [9], and the other assumed no plasmaspheric density. These runs are `A-CHAIM (NPSM)` and `A-CHAIM (no NPSM)`. As seen in Figure 2, the change in DCBs with and without the NPSM was small, with a median difference of less than 0.5 TECU across all stations.

Two more test runs were conducted by assimilating Madrigal vTEC maps by integrating the electron density from the
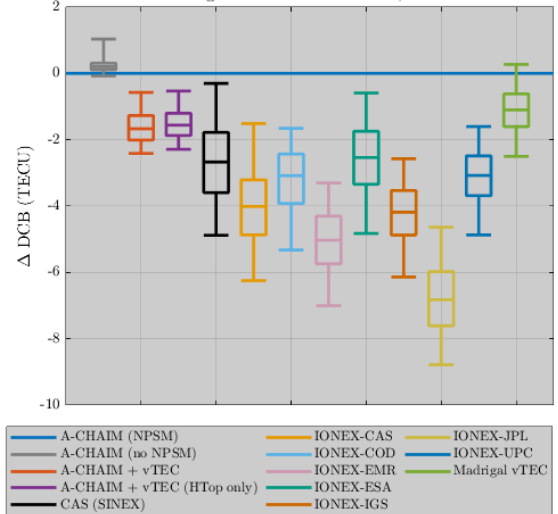


**Figure 2.** A comparison of DCB estimation techniques during the August 20th through October 10th 2022 test period. The outer limits at the $5^{th}$ and $95^{th}$ percentiles. The CAS (SINEX) values were taken from the published SINEX files, and so only includes 76/660 stations.

ground up to GPS satellite altitude at every grid point. Any vTEC with an associated error greater than 5 TECU was rejected as an outlier, and not assimilated. In `A-CHAIM + vTEC`, the vTEC was assimilated as any other data. `A-CHAIM + vTEC(HTop)` was configured to preferentially change the topside thickness to match Madrigal, when compared to `A-CHAIM + vTEC`.

## 4 Discussion

Figure 3 allows us to compare the effects of Madrigal vTEC assimilation on the model. In the first column we have the model DCBs compared to those estimated by levelling to the Madrigal vTEC maps. This can be compared with the second column, which is the mean difference in modelled vTEC less Madrigal vTEC over the entire test period. It is clear that in regions where `A-CHAIM (NPSM)` underestimates Madrigal vTEC, it overestimates DCBs. The two lower rows, where vTEC was assimilated, show a much more even vTEC map over Europe and America.

The third column shows the mean difference between the model and ionosonde NmF2. While the `A-CHAIM (NPSM)` and `A-CHAIM + vTEC(HTop)` runs show very similar results, the `A-CHAIM + vTEC` run almost universally overestimates NmF2. During the day at mid-latitudes this is an error of single digit percentage. At nighttime, the error in NmF2 is on the order of 20%. By forcing `A-CHAIM + vTEC` to match the Madrigal vTEC, it was possible to bring the DCBs into broad agreement, at the cost of overestimating NmF2 significantly.
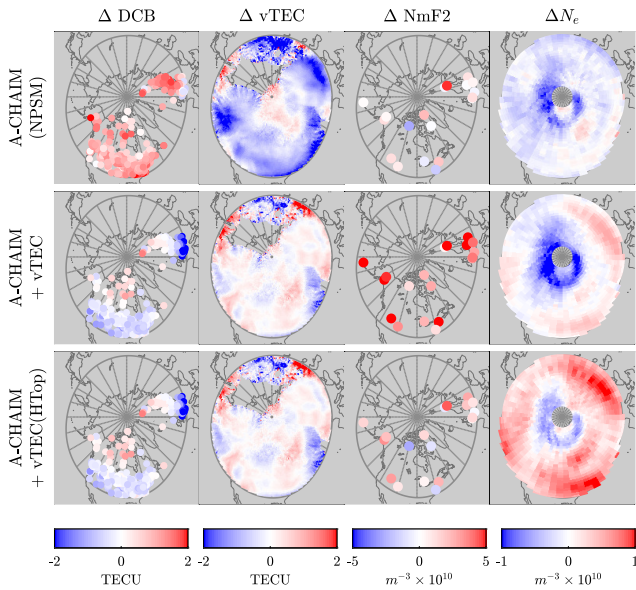
**Figure 3.** Global comparisons of each of the A-CHAIM test runs, averaged over the whole test period from August 20th through October 10th.

The final column shows the average bias between the model, and in-situ measurements from the DMSP satellites. At lower latitudes, the differences are significant. The `A-CHAIM + vTEC` run shows a slight enhancement in electron density, and the `A-CHAIM + vTEC(HTop)` run shows global overestimation on the order of $1 \times 10^{10} m^{-3}$. This is an overestimation of 35% when compared to average in-situ measurements during the test period. A-CHAIM assimilates ionosonde measurements of foF2, hmF2, foF1 and bottomside thickness, and so the overall shape of the bottomside ionosphere is well constrained. The topside is the most weakly observed region of the ionosphere in A-CHAIM, and would be the most likely source of a systematic underestimation. When the topside is forced to match Madrigal vTEC, while keeping the bottomside consistent with ionosonde measurement, the resulting densities do not match observations.

## 5 Conclusion

The Rao-Blackwellised particle filter technique used in A-CHAIM is able to produce stable estimates of receiver DCBs. The DCBs produced in this way show systematic biases relative to the DCBs estimated through other means, ranging from 1.5 TECU to 7 TECU. A plasmasphere model was added to A-CHAIM, which reduced the bias by 0.4 TECU. Two additional test runs of A-CHAIM were conducted, where vTEC measurements from Madrigal were assimilated. Both of these runs produced vTEC and DCBs in broad agreement with the Madrigal values. One run placed no constraints on A-CHAIM, which resulted in a global overestimation of NmF2 ranging from $< 10\%$ during the day to over 20% at night. The second run was configured to force A-CHAIM to match Madrigal vTEC without affecting NmF2. This resulted in a signifi-

cant overestimation of topside electron density on the order of 30%. These tests suggest that it is not currently possible for A-CHAIM to simultaneously produce DCBs in agreement with other sources, while also reproducing electron densities in agreement with data. The electron density produced by A-CHAIM is consistent with observations at all altitudes up to 800 km, the altitude of the DMSP satellites. It is unlikely that any further refinement of the topside would produce a change greater than 1 TECU.

## References

[1] B. Reid, D. R. Themens, A. M. McCaffrey, P. T. Jayachandran, M. G. Johnsen, and T. Ulich, "A-chaim: Near-real-time data assimilation of the high latitude ionosphere with a particle filter," preprint. [Online]. Available: doi.org/10.1002/essoar.10511639.1

[2] D. R. Themens, P. T. Jayachandran, R. B. Langley, J. W. Macdougall, and M. J. Nicolls, "Determining receiver biases in gps-derived total electron content in the auroral oval and polar cap region using ionosonde measurements," *GPS Solut.*, vol. 17, no. 3, p. 357–369, Jul 2013.

[3] *IONEX: The IONosphere Map EXchange Format Version 1.1*, Sep 2017. [Online]. Available: https://gssc.esa.int/wp-content/uploads/2018/07/ionex11.pdf

[4] D. Roma-Dollase, M. Hernández-Pajares, A. Krankowski, K. Kotulak, R. Ghoddousi-Fard, Y. Yuan, Z. Li, H. Zhang, C. Shi, C. Wang, J. Feltens, P. Vergados, A. Komjathy, S. Schaer, A. García-Rigo, and J. M. Gómez-Cama, "Consistency of seven different gnss global ionospheric mapping techniques during one solar cycle," *Journal of Geodesy*, vol. 92, no. 6, pp. 691–706, Jun 2018.

[5] W. Rideout and A. Coster, "Automated gps processing for global total electron content data," *GPS Solutions*, vol. 10, no. 3, pp. 219–228, Jul 2006.

[6] J. Vierinen, A. J. Coster, W. C. Rideout, P. J. Erickson, and J. Norberg, "Statistical framework for estimating gnss bias," *Atmospheric Measurement Techniques*, vol. 9, no. 3, pp. 1303–1312, 2016.

[7] A. Doucet and A. Johansen, "A tutorial on particle filtering and smoothing: Fifteen years later," *Handbook of Nonlinear Filtering*, vol. 12, 01 2009.

[8] P. J. van Leeuwen, H. R. Künsch, L. Nerger, R. Potthast, and S. Reich, "Particle filters for high-dimensional geoscience applications: A review," *Quarterly Journal of the Royal Meteorological Society*, vol. 145, no. 723, pp. 2335–2365, 2019.

[9] Jakowski, Norbert and Hoque, Mohammed Mainul, "A new electron density model of the plasmasphere for operational applications and services," *J. Space Weather Space Clim.*, vol. 8, p. A16, 2018.